scientific reports

Check for updates

OPEN

Amplifying the photovoltaic properties of tetrathiafulvalenes based materials by incorporation of small acceptors: a density functional theory approach

Muhammad Khalid[1,2]✉, Ayesha Tariq[1,2], Ataualpa A. C. Braga[3], Rajeh Alotaibi[4] & Suvash Chandra Ojha[5]✉

Currently, polycyclic aromatic compounds in organic solar cells (OSCs) have gained substantial consideration in research communities due to their promising characteristics. Herein, polycyclic aromatic hydrocarbons (PAHs) core-based chromophores (TTFD1-TTFD6) were designed by structural modifications of peripheral acceptor groups into TTFR. The density functional theory (DFT) and time dependent density functional theory (TD-DFT) calculations were carried out at B3LYP/6-311G (d, p) functional to explore insights for their structural, electronic, and photonic characteristics. The structural modulation unveiled notable electronic impact on the HOMO and LUMO levels across all derivatives, leading to decreased band gaps. All the designed compounds exhibited band gap ranging from 2.246 to 1.957 *eV*, along with wide absorption spectra of 897.071-492.274 *nm*. An elevated exciton dissociation rate was observed due to the lower binding energy values (E_b = 0.381 to 0.365 *eV*) calculated in the derivatives compared to the reference (E_b = 0.394 *eV*). Furthermore, data from the transition density matrix (TDM) and density of states (DOS) also corroborated the effective charge transfer process. Comparable results of V_{oc} for reference and designed chromophores were obtained *via* $HOMO_{donor}$—$LUMO_{PC71BM}$. The declining V_{oc} order values was noted as TTFD5 > TTFD6 > TTFD4 > TTFD3 > TTFD2 > TTFD1 > TTFR. Interestingly, TTFD5 was found with the smallest energy gap and highest absorption value, resulting in better charge transference among all the derivatives. The results illustrated that the modification in indenofluorene based chromophores with end-capped small acceptors proved to be a significant approach in achieving favorable photovoltaic properties.

Keywords Indenofluorene-tetrathiafulvalenes, Small acceptors, Photovoltaic materials, A-π-A configuration, Open circuit voltage

Nowadays, organic solar cells (OSCs) have garnered considerable interest owing to their simple processing, remarkable mechanical flexibility, and a notable rise in their power conversion efficiency (PCE) to above 18%[1–4]. The progress of organic photovoltaics (OPVs) is accomplished by tuning the optoelectronic characteristics of organic compounds[5]. OSCs usually employ either fullerene or non-fullerene (NF) based compounds as the primary types of organic materials[6]. During the previous two decades, fullerene-based electron acceptors (FAs) are seen with significant progress in the field of solar cells[7]. Fullerene-based OSCs have become increasingly valued in the market due to their lower molecular weight, cost-effectiveness, reproducibility, and ease of processing.

[1]Institute of Chemistry, Khwaja Fareed University of Engineering & Information Technology, Rahim Yar Khan 64200, Pakistan. [2]Centre for Theoretical and Computational Research, Khwaja Fareed University of Engineering & Information Technology, Rahim Yar Khan 64200, Pakistan. [3]Departamento de Química Fundamental, Instituto de Química, Universidade de São Paulo, Av. Prof. Lineu Prestes, 748, São Paulo 05508-000, Brazil. [4]Department of Chemistry, College of Science, King Saud University, Riyadh 11451, Saudi Arabia. [5]Department of Infectious Diseases, The Affiliated Hospital of Southwest Medical University, Luzhou 646000, China. ✉email: khalid@iq.usp.br; muhammad.khalid@kfueit.edu.pk; suvash_ojha@swmu.edu.cn

However, the drawbacks of these solar cells include limited light absorption, weak acceptor capabilities, and low tunable energy levels[8].

In the modern era, researchers are intrigued by using non-fullerene acceptors in photovoltaic applications which is driven by their versatility, cost-effectiveness, higher energy conversion efficiency and transparency[9–11]. The NF small molecule acceptors demonstrate strong optical absorption, extending their absorption range into the infrared region of spectra[12–14]. Non-fullerene organic solar cells (NF-OSCs) are classified into two groups: small molecular acceptors (SMAs) and polymer solar cells (PSCs)[15–17]. Organic solar cells are built upon the foundational design of inorganic solar cells, replacing n-type and p-type materials with acceptor and donor type components, respectively, that are more significant[18,19]. From last two decades, significant efforts have been devoted to develop polymer bulk heterojunction (BHJ) solar cells (SCs) based on fullerene acceptors and polymeric donors, resulting in an efficacy improvement to 8.3%.[20] On the other hand, SMAs exhibit improved photovoltaic characteristics than PSCs because of enhanced reproducibility, simplified purification processes, and a unique molecular structure[21–23]. The PCEs of organic photovoltaics is boosted through the increased molar absorption coefficient of NFAs[24]. The NFAs possess broader absorption spectra, elevated absorption coefficients, flexible power levels, and organized packing arrangements in contrast to fullerene-based ones[25,26]. Moreover, NFAs offer a wide array of structural configurations that are recognized for their high efficiency in promoting intramolecular charge transfer (ICT)[27]. These include various structural configurations such as donor-acceptor-donor[28], acceptor-donor-acceptor[29], and acceptor-donor-acceptor-donor-acceptor etc. Over the past few years, the utilization of NFAs has facilitated the development of OSCs, achieving 16% PCE with A-D-A type configuration[30]. The NFA namely ITIC, exhibited an A-D-A configuration, comprises two electron-withdrawing groups characterized by a donor core is repoted with significant efficacy[31]. It is commonly observed that modifying molecular properties such as crystallinity, energy levels, and optical absorption capability through structural adjustments can significantly enhance the performance of NFA-based devices[32–34]. Literature is flooded with many examples in which compounds with central donor core having electron withdrawing bracing units are successfully synthesized for high efficacy organic solar cells[35,36].

A novel synthesized compound dcIF-TTF is taken from literature and utilized as reference chromophore to designed new derivatives for current study[37] This compound is part of a class called indenofluorene extended tetrathiafulvalenes (IF-TTFs). These compounds are synthesized by extending the indenofluorene core (IF), which is a type of polycyclic aromatic hydrocarbon (PAH), with tetrathiafulvalene (TTF) units. PAHs are important in organic optoelectronic materials due to their extensive π-conjugation and charge delocalization[38]. The chromophore dcIF-TTF was made by attaching a dicyano indenofluorene core (dcIF) to TTF units. This design aimed to create an effective photovoltaic material that shows a significant bathochromic shift, lower excitation energies, a narrow band gap with higher power conversion efficiency. The name of reference chromophore (dcIF-TTF) is changed as TTFR in current study. Based on these properties, six new derivatives with A-π-A architecture of TTFR have been designed in this research abbreviated as TTF1-TTF6. After designing of tetrathiafulvalenes based compounds, their photovoltaic properties were investigated through DFT approach. The structural modification involves the attachment of various strong electron-withdrawing end-capped small acceptors around the central unit π-bridge to examine the impact of these end groups on the photovoltaic characteristics of newly designed compounds utilized as solar cell materials. Earlier research has demonstrated that introducing the terminal moieties during the designing of compounds is a successful method for achieving elevated optoelectronic attributes and noteworthy PCE in NFA[39]. It is anticipated that aforementioned designed derivatives based on dcIF-TTF could serve as effective materials for photovoltaic OSCs.

Results and discussion

The quantum chemical investigation focused on a comprehensive computational analysis of newly designed fullerene free organic photovoltaic materials. The literature contains numerous reports where small entities such as thiophene, imidazole, selenophene etc. have been employed to enhance the charge transfer properties of organic materials[40]. To achieve this, A-D-A configuration is selected as the parent chromophore, containing a donor core, with terminal electron-withdrawing groups (-CN) on either side[37]. Hence, a set of donor photovoltaic compounds, TTFD1-TTFD6 is designed, via structural modulation at the acceptor part of TTFR with thiophene-based small acceptors (A1-A6), aiming to attain highly efficient OSCs. The optimized structures of aforementioned chromophores are demonstrated in Figure S2 while their structural illustration is portrayed in Fig. 1. The IUPAC names of TTFR-TTFD6 compounds and their utilized acceptors (A1-A6) are displayed in Table S9 and S1, respectively. Moreover, the cartesian coordinates of designed chromophores are presented in Tables S1-S7.

Electronic structure

Frontier molecular orbitals (FMOs) analysis is an eminent method to assess the potential of intermolecular charge transfer (ICT) in the studied molecules TTFR and TTFD1-TTFD6[41,42]. The FMOs offers insights into a molecule reactivity potential through electronic transitions from HOMO to LUMO[43]. Additionally, they are crucial for influencing solar cell properties, enable them to transport charges efficiently and facilitate the flow of electric current[44,45]. The band gap between HOMO-LUMO is a key factor to determine the exciton dissociation energy. Therefore, we have computed the energy levels of FMOs of TTFR and TTFD1-TTFD6 using DFT/B3LYP/6-311G(d, p) method, and the findings are detailed in Table 1.

The computed HOMO/LUMO values for TTFR were found to be -5.50/-2.59 eV, while the designed molecules TTFD1-TTFD6 exhibited values of -5.39/-3.15, -5.42/-3.22, -5.44/-3.29, -5.45/-3.34, -5.58/-3.86 and −5.52/-3.56 eV, respectively. The energy gap (ΔE) of the reference molecule was determined to be 2.91 eV. Whereas, for the designed molecules, this gap was measured at 2.25, 2.20, 2.16, 2.11, 1.72, 1.96 eV, respectively, as depicted in Table 1. All the designed derivatives (TTFD1-TTFD6) exhibited narrow bandgaps compared to

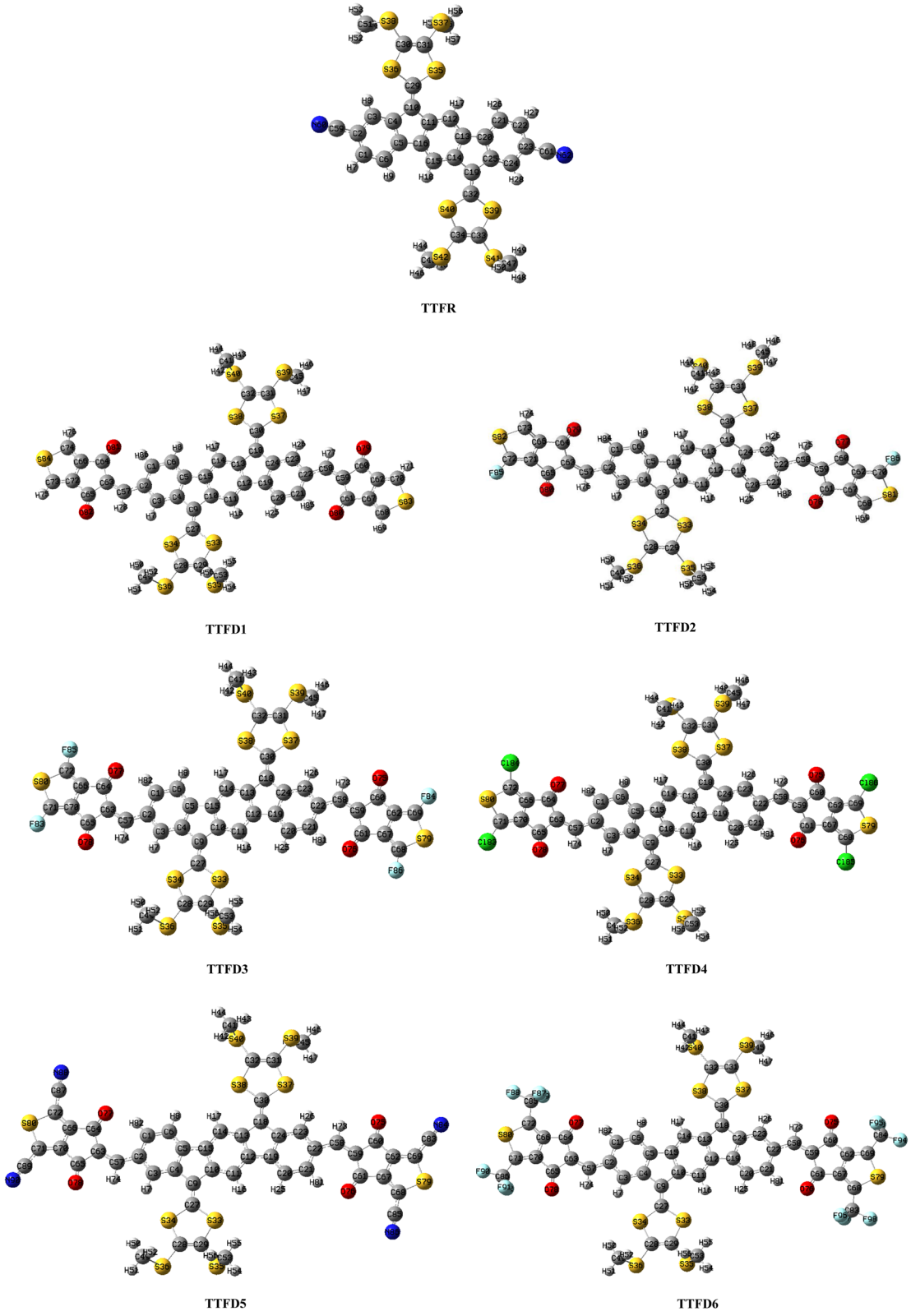

Figure 1. Optimized structures of TTFR and TTFD1-TTFD6

the reference compound. This confirms the effectiveness of our design strategy for synthetic pursuits. Among the designed compounds, TTFD5 possess the smallest energy band gap value 1.72 *eV* as compared to others, due to the incorporation of effective terminal acceptor groups namely 5-methylene-4,6-dioxo-3-phosphino-5,6-dihydro-4 H-cyclopenta[c]thiophene-1-carbonitrile (A5). This band gap increases to 1.96 in TTFD6 when

Compounds	HOMO	LUMO	ΔE
TTFR	-5.50	-2.59	2.91
TTFD1	-5.39	-3.15	2.25
TTFD2	-5.42	-3.22	2.20
TTFD3	-5.44	-3.29	2.16
TTFD4	-5.45	-3.34	2.11
TTFD5	-5.58	-3.86	1.72
TTFD6	-5.52	-3.56	1.96

Table 1. Calculated energies (E) and energy gap (ΔE) for TTFR and TTFD1-TTFD6. Band gap = $E_{LUMO} - E_{HOMO}$, units in eV.

cyano (-CN) groups were replaced with carbon trifluoride (-CF_3) moieties at peripheral acceptors A6. This might because of stronger resonance effect exhibited by the cyano group that delocalizes electron density more efficiently than inductive effect of the nitro group. TTFD4 exhibits smaller band gap (2.11 eV) than TTFD3 (2.16 eV), as chloro functions withdraws electron density less effectively from the π-conjugated system compared to fluoro moieties at terminal acceptors in TTFD3. Similarly, TTFD1 featuring 5-methylene-4 H-cyclopenta[c] thiophene-4,6(5 H)-dione showing energy gap of 2.25 eV. This energy gap lowers to 2.20 eV in TTFD2 due to the addition of fluoro groups at terminal acceptors. Overall, the decreasing trend of band gap is as follows: TTFD6 < TTFD5 < TTFD4 < TTFD3 < TTFD2 < TTFD1 < TTFR. The FMOs help us understand the charge transference phenomenon examined in TTFR and TTFD1-TTFD6. Figure 2 depicts that in HOMO of TTFR charge density is primarily resides on entire molecule except tetrathiafulvalene moiety and end capped cyano acceptors. In the LUMO, the charge density mostly spreads across the entire compound except for the tetrathiafulvalene part and the -CH_3 group. The FMOs of HOMO-1/LUMO + 1 and HOMO-2/LUMO + 2 are depicted in Figure S3. The electronic density for all designed compounds is majorly focused on the central core (π-linker) for HOMO. For LUMO, the charge density covers the entire compound except tetrathiafulvalene and -CH_3 groups.

Optical properties

The optoelectronic behavior of investigated compounds (TTFR and TTFD1-TTFD6) is computed using time dependent density functional theory (TD-DFT) approaches in gaseous and solvent phases. The B3LYP/6-311G(d, p) functional is used to investigate red or blue shifts in the UV-Visible spectrum of all the designed chromophores. The results based on maximum absorption (λ_{max}), excitation energy (E), oscillator strength (f_{os}), and molecular orbital transitions are presented in Tables S10, S11 and S12 for all entitled compounds. All designed molecules TTFD1-TTFD6 show higher degree of red shift in the absorption spectra than reference compound.

Normally, a shift towards longer wavelength in the absorption spectrum indicates greater photovoltaic efficiency[46]. The difference in absorption peak illustrates the influence of solvent; i.e., the elevated absorption maxima in the toluene indicated a faster rate of solubility for acceptor materials in the solvent media compared to the gaseous state (see Fig. 3)[47]. TTFD5 exhibits the highest absorption rate due to strong electron-withdrawing effect of its two cyano groups situated on the terminal acceptors. The absorption trend in toluene is decreases in the following sequence: TTFD5 (897.071) > TTFD6 (778.648) > TTFD4 (714.359) > TTFD2 (681.456) > TTFD3 (663.798) > TTFD1 (664.723) > TTFR (492.274), correlating inversely with E_x. Excitation energy offers another avenue to estimate the effectiveness of OSCs. Generally, less excitation energy values indicate higher power conversion efficiency PCE in OSCs[48]. The excitation energies of all examined the compounds are listed as follows: TTFR (2.519) > TTFD3 (1.868) > TTFD1 (1.865) > TTFD2 (1.819) > TTFD6 (1.592) > TTFD4 (1.736) > TTFD5 (1.382) in nm. The λ_{max} values calculated for all examined molecules in the gaseous phase are almost same with those observed in the solvent phase. Above findings indicate better optoelectronics properties in all designed compounds compared to TTFR. This emphasizes the effectiveness of structural modeling the parent molecule with robust acceptor units, resulting in chromophores with narrower bandgaps and broader absorption spectra, thus paving the way to develop promising OSCs materials.

Density of state (DOS)

Density of states (DOS) investigation was conducted using the aforedescribed functional and basis set to support the results of FMOs, demonstrating a comparable relationship between them. DOS is conducted to reveal the electron density distribution across FMOs in the form of percentage composition for all entitled compound[49]. The DOS pictographs depicted in Fig. 4 illustrate how the electron-withdrawing potential of acceptor groups causes shifts in charge density around the HOMO and LUMO. For further study DOS, all designed compounds are split into two fragments as π-bridge (central core) and acceptor (peripheral moieties) which are presented by green and red lines, correspondingly. The central spacer part is connected to the terminal acceptor groups which ensure good intermolecular charge transference within entitled compounds. In DOS pictographs, the left side values denote HOMOs while right side results signifies the LUMOs along x-axis and the distance between HOMOs and LUMOs denote the energy gap[50].

In the case of reference compound (TTFR)π-spacer contribution for HOMO and LUMO is 100.0%, and 94.1% respectively. While the acceptor contribution is 0.0%, to the HOMO and 88.6, 5.9% to the LUMO for TTFR,

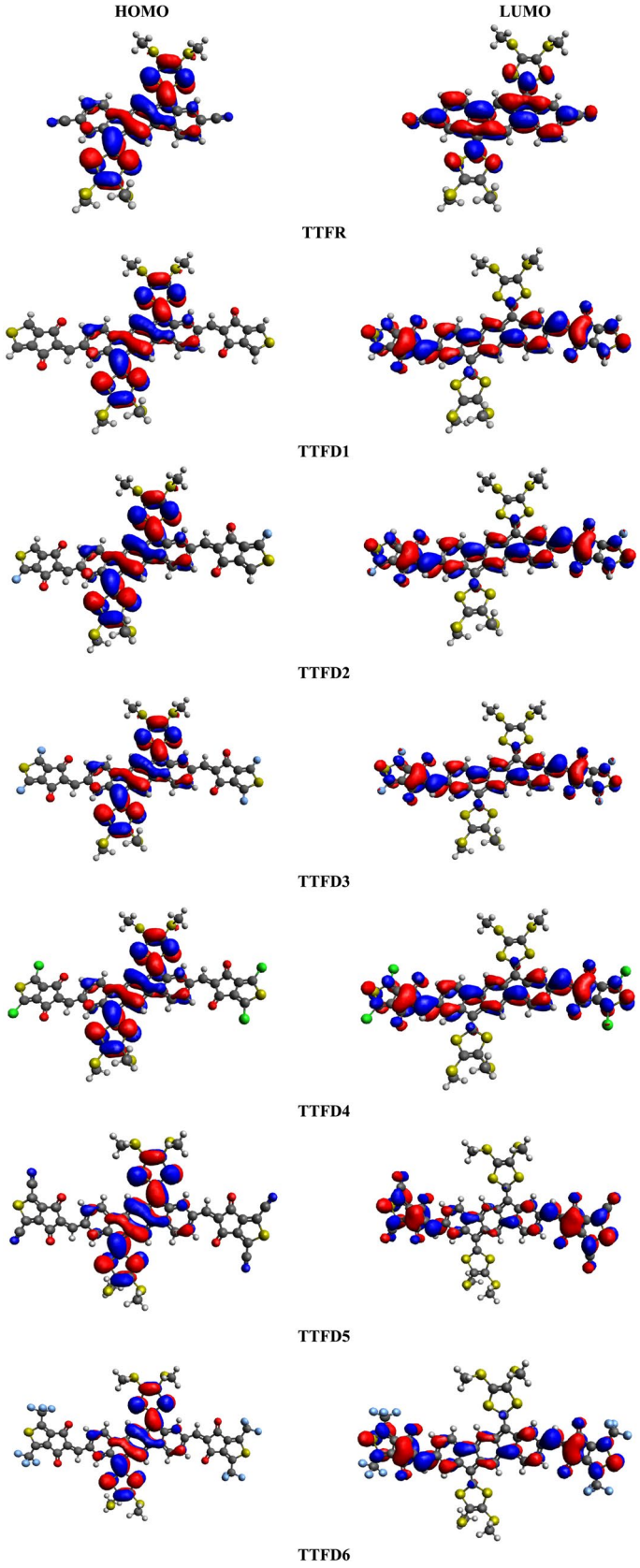

Figure 2. HOMOs and LUMOs of the designed chromophores (TTFR-TTFD6).

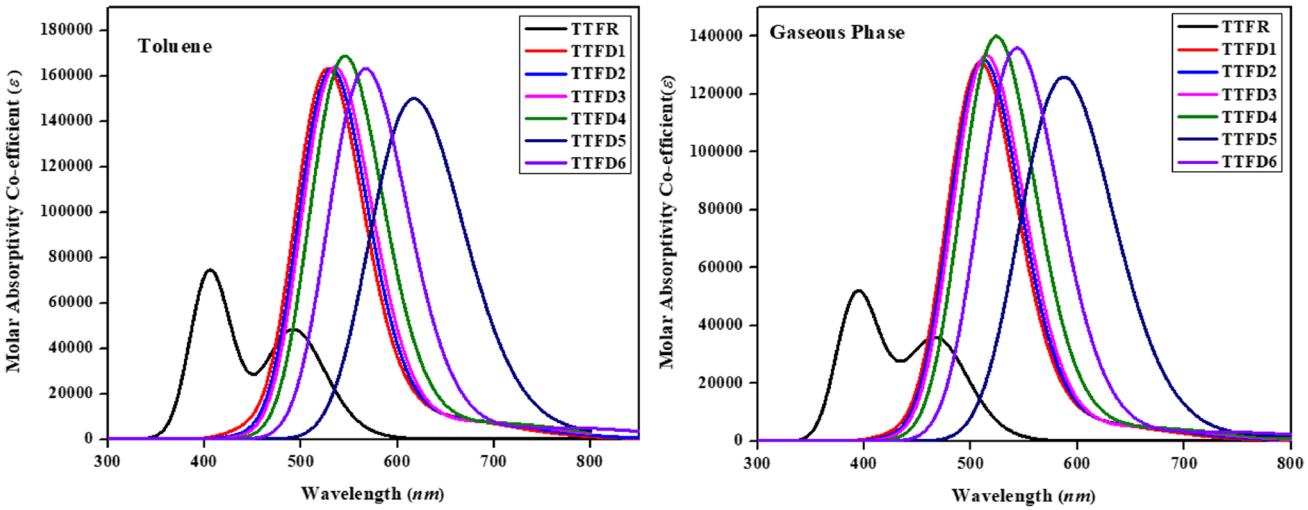

Figure 3. Absorption spectra of TTFR and TTFD1-TTFD6 in toluene and gas phase.

respectively. Herein, acceptor showed electronic distribution pattern as 61.3%, 62.0%, 62.5%, 65.3%, 79.6% and 70.1% to LUMO while 99.9% to HOMO for TTFD1-TTFD6, respectively. Similarly, π-spacer participated 38.7%, 38.0%, 37.5%, 34.7%, 20.4% and 29.9% to LUMO whereas 0.1% to HOMO for TTFD1-TTFD6, respectively as shown in Table S13. These results show that the HOMO orbitals are mostly found on the spacer parts and the LUMO orbitals are mainly found on the acceptor moieties in the designed compounds.

In all the examined chromophores (TTFD1-TTFD6), the highest charge density on the LUMO is observed within the span of -3 to -3.5 *eV* energy, whereas the maximum density on the HOMO is observed between −7 to -8 *eV*. The graphs for DOS strongly supported the FMOs diagram, suggesting significant flow of internal charge in all the designed derivatives. In nutshell, the charge distribution pattern demonstrates that an efficient charge density is transferred from *π*-spacer to acceptor moieties, making it a good candidate for solar cell applications.

Transition density matrix (TDM)

The Transition Density Matrix (TDM) analysis is used to analyze the transfer of charge density within molecular systems[51]. It is utilized to elucidate the electronic excitations occurring from S_0 to S_1 excited state. It furnishes a spatial representation for identifying the interaction of acceptor and donor moiety in excited state and hole-electron localization[52]. The B3LYP/6-311G(d, p) method was employed to analyze transitions in the excited state. The role of hydrogen in charge density estimations is negligible due to its minimal impact on overall transitions. For suitability, the compound is divided into acceptor (A) and π-spacer. The TDM plots are shown in Fig. 5. The electron coherence is detected in all the examined (TTFD1-TTFD6) chromophores; π-spacer effectively transfers the electron density which is accepted by efficient acceptor groups. Based on the sequence TTFD5 > TTFD6 > TTFD4 = TTFD3 > TTFD3 > TTFD1 > TTFR, there's a notable interaction coefficient between acceptor and donor groups. Among all, TTFD5 has shown improved charge transference from π-linker to end capped acceptor moieties without any charge trapping owing to π-π^* transition and the π-conjugation. Therefore, TTFD5 has auspicious charge delocalization potential. Therefore, as a result of this phenomenon, the flow of electron density persists throughout the entire molecule efficiently.

Exciton binding energy (E_b)

The exciton binding energy (E_b) is a fundamental parameter to elucidate the efficacy and optoelectronic characteristics of organic photovoltaic solar cells[53]. It elucidates the relation between the Columbic attraction of hole and electrons within the material. E_b is the minimum energy needed to generate free electron and hole carriers[54]. E_b directly influences charge generation, transport, and recombination processes, as well as the probability of exciton dissociation at the donor-acceptor interface, thereby impacting overall device performance. A decreased binding energy facilitates the disruption of the Columbic forces between the electron and hole, therefore aiding in exciton delocalization and enhancing transfer of charge. Furthermore, a smaller ΔE value results in increased exciton dissociation and reduced energy loss. It is experimentally calculated by Eq. 1.[55]

$$E_b = E_{H-L} - E_{opt} \tag{1}$$

In the above equation, $E_{L\text{-}H}$ E_{H^-L} and E_x denote the molecular orbitals band gap and energy of excitations, correspondingly. Upon reviewing Table 2, it is noted that all designed molecules (TTFD1- TTFD6) exhibit lower E_b values compared to reference compound (TTFR), indicating enhanced exciton dissociation in the excited state. Among all, TTFD3 exhibits the lowest E_b value due to the introduction of efficient electron capturing acceptor moieties at the terminals aids in dropping Columbic forces, thereby facilitating easier dissociation[56]. The decreasing order of E_b all designed chromophores is TTFR > TTFD2 > TTFD1 > TTFD4 > TTFD6 > TTFD5 > TTFD3.

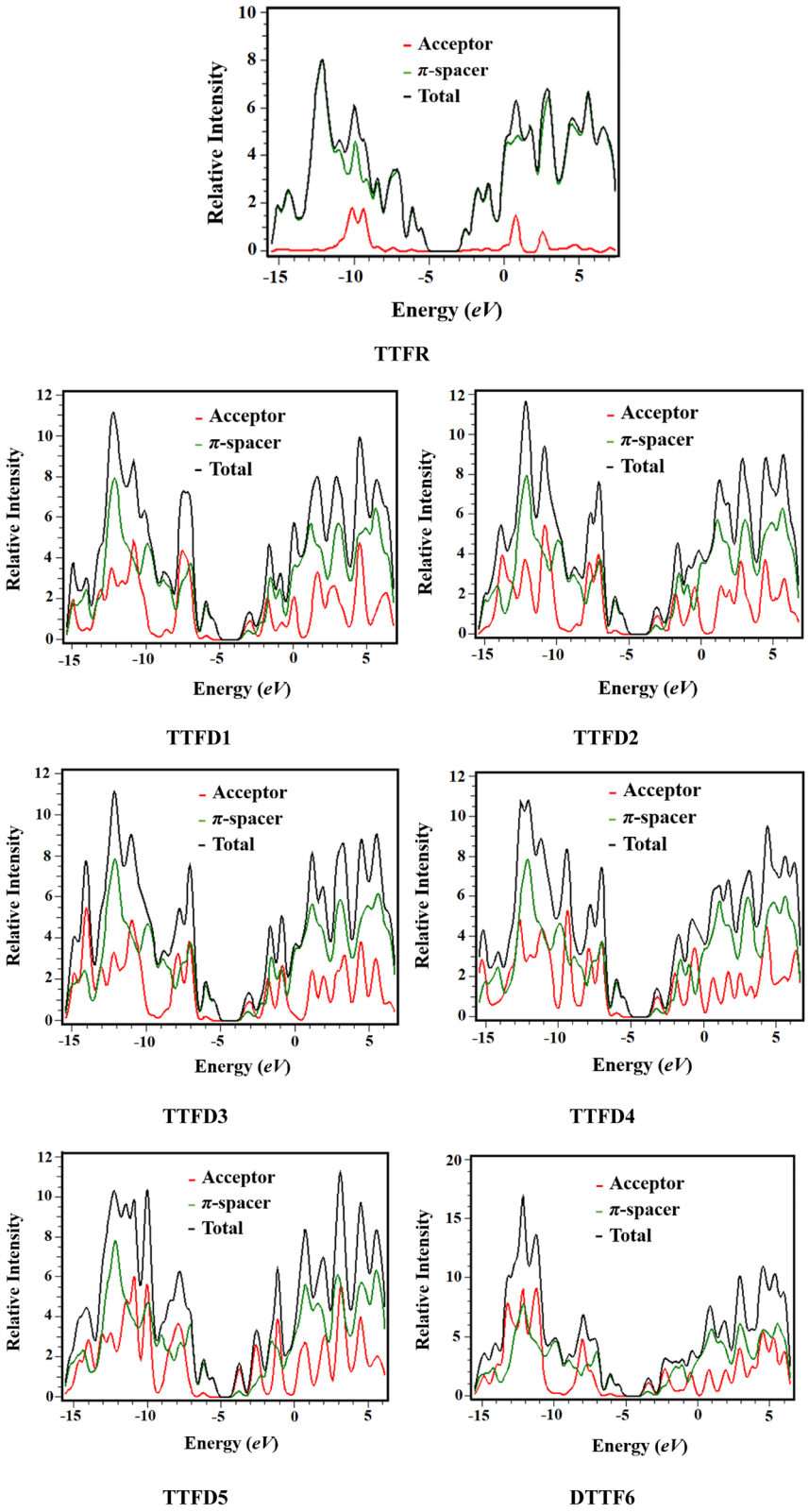

Figure 4. The pictographs of density of state for TTFR and TTFD1-TTFD6.

Electron hole analysis

The analysis of holes and electrons aids to determine how charge carriers and excitations behave in photovoltaic materials (TTFR- TTFD6)[57]. Hole-electron analysis is executed by using Multiwfn 3.8 software as shown in Fig. 6. In this investigation, analysis of hole-electron interactions is conducted by B3LYP/6-311G (d, p) method

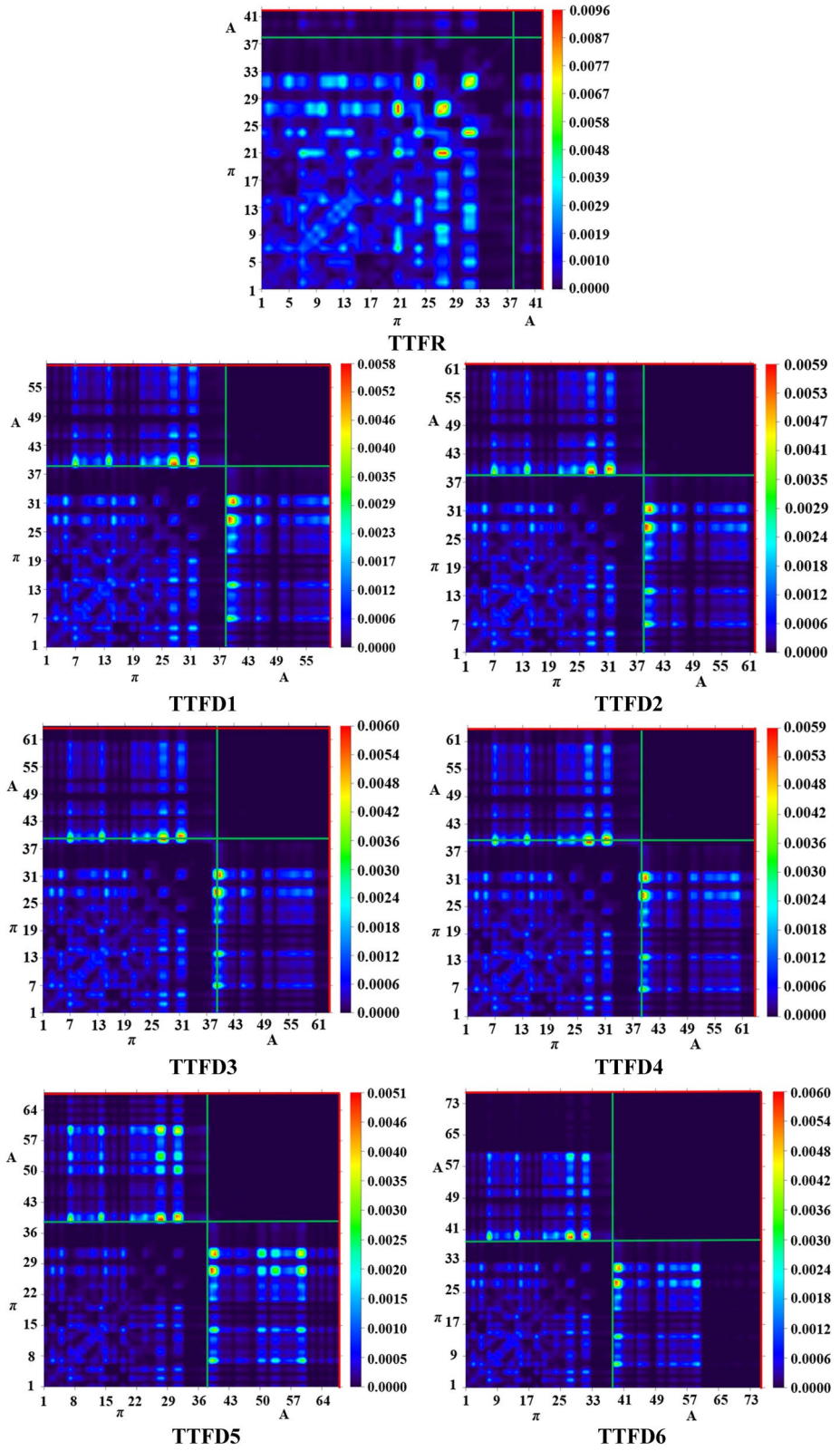

Figure 5. TDM heat maps of TTFR and TTFD1 - TTFD6 compounds.

to comprehend the charge transfer in the designed molecules. Heat maps demonstrate that in TTFR, a hole is created at the carbon atom (C14) and electronic cloud at carbon atom (C21) of π-linker. Similarly, in TTFD1, TTFD2 and TTFD3 substantial hole potential is found at C10 of π-linker and dense charge density is present at C39 of terminal acceptors. While greater hole density in chromophores (TTFD4 and TTFD5) is present at C14

Compounds	$E_{H\text{-}L}$	E_{opt}	E_b
TTFR	2.913	2.519	0.394
TTFD1	2.246	1.865	0.381
TTFD2	2.201	1.819	0.382
TTFD3	2.157	1.868	0.289
TTFD4	2.111	1.736	0.375
TTFD5	1.718	1.382	0.336
TTFD6	1.957	1.592	0.365

Table 2. Calculated E_b TTFR and TTFD1- TTFD6 compounds. Units in eV.

of π-linker. In TTFD6 greater hole density is located at C14 and significant electron density is observed at C39 and C40 of end capped terminal acceptors. So, it is evident from maps, hole densities are present across different atoms of the π-spacer, accompanied by charge transference in the acceptor part.

Reorganization energy

Reorganization energy is an important approach to analyze molecular structure influences the molecule's charge transference capacity. Moreover, it assists to comprehend the charge transition from donor to acceptor segment of a molecule. Compounds with a small RE value displayed enhanced photovoltaic properties, reflecting greater charge flexibility[58]. Therefore, to comprehend the charge mobility, the hole mobility (λ_h) and electron mobility (λ_e), of the examined chromophores, the RE was computed using the B3LYP/6-311G(d, p) functional as shown in Table 3.

The computed RE values of the hole for TTFR is -0.00059988 eV and for TTFD1-TTFD6 are 0.10506045, -0.00020501, -0.00033909, -0.00023788, -0.00046074, and −0.00080507 eV, correspondingly. The decreasing trend of λ_h for the investigated compounds is TTFD1 > TTFD2 > TTFD4 > TTFD3 > TTFD5 > TTFR > TTFD6. The calculated value of λ_e for reference is 0.00066671 eV whereas for TTFD1-TTFD6 are 0.10532127, 0.00066671, 0.00013195, 0.0001314, 0.00010953, -0.00001172, and −0.00007836 eV, respectively. The declining order of λ_e for designed compounds is TTFD1 > TTFR > TTFD3 > TTFD4 > TTFD2 > TTFD5 > TTFD6. The analysis reveals that all derivatives, exhibit lower λ_h values, suggesting a superior hole transport. This investigation underscores the enhanced charge-transport efficiency of these chromophores, marking them as promising candidates for OSCs.

Photovoltaic properties

The open circuit voltage (V_{oc}) analysis serves as a crucial parameter for evaluating device performance, manifesting at zero current level. V_{oc} represents the highest electrical potential output by a device when no current is flowing[59]. V_{oc} values are influenced by various factors, including solar cell temperature, light intensity, material types, energy levels, and electrode functionalities[60]. A higher V_{oc} value correlates with a higher fill factor (FF), which is pivotal in assessing solar cell efficiency. V_{oc} are further elucidated based on HOMO/LUMO energy levels. The possibility of transfer of electron from the HOMO level of donor to the LUMO level of acceptor increases, enhancing V_{oc} when the acceptor's LUMO is resided at lower energy. The V_{oc} for all the designed molecules is calculated by blending it to the $PC_{71}BM$ polymer (acceptor nature). The V_{oc} is obtained by the energy difference between the HOMO of the donor (π-conjugated molecule) and the LUMO of the acceptor ($PC_{71}BM$ polymer), considering energy dissipation during photo-charge generation[61]. Equation 2[62] was utilized to ascertain V_{oc} as depicted in Table S14, where the computed values are tabulated.

$$V_{OC} = \left(\left|E^{D}{}_{HOMO}\right| - \left|E^{A}{}_{LUMO}\right|\right) - 0.3 \tag{2}$$

The V_{oc} of reference material (TTFR) is 1.771 V, and for designed compounds (TTFD1- TTFD6) is 1.662, 1.692, 1.714, 1.723, 1.849 and 1.789 V. These values indicate that TTFD5 shows the highest V_{oc} value, attributed to a significant red shift (λ_{max}) in the absorption spectra induced by terminal efficient acceptor moieties. Moreover, TTFD5 has the potential to serve as a more competent power-generating molecule in future photovoltaic cells. All derivatives exhibit comparable V_{oc} values to the reference molecule (TTFR). The declining V_{oc} order for the designed chromophores is TTFD5 > TTFD6 > TTFD4 > TTFD3 > TTFD2 > TTFD1. Figure 7 illustrates a graphical depiction of the V_{oc} values.

Observations indicate that with increasing V_{oc}, the PCE and ICT also increase. Above mentioned results demonstrates that TTFD5 showcased the highest energy and V_{oc} values, making it a dependable choice for boosting the efficiency of solar devices.

Conclusion

In this study, a sophisticated quantum chemical approach is utilized to understand the photovoltaic characteristics of indenofluorene-tetrathiafulvalenes compounds. By structural modification of TTFR molecules, six thiophene based small acceptor chromophores (TTFD1-TTFD6) were designed. The results indicated that structural modifications with effective electron-withdrawing components notably improved the photovoltaic characteristics of all derivatives as compared to the reference TTFR. Notably, all the entitled chromophores exhibit narrow band gaps (2.246 to 1.957 eV) compared to TTFR (2.913 eV), suggesting facile

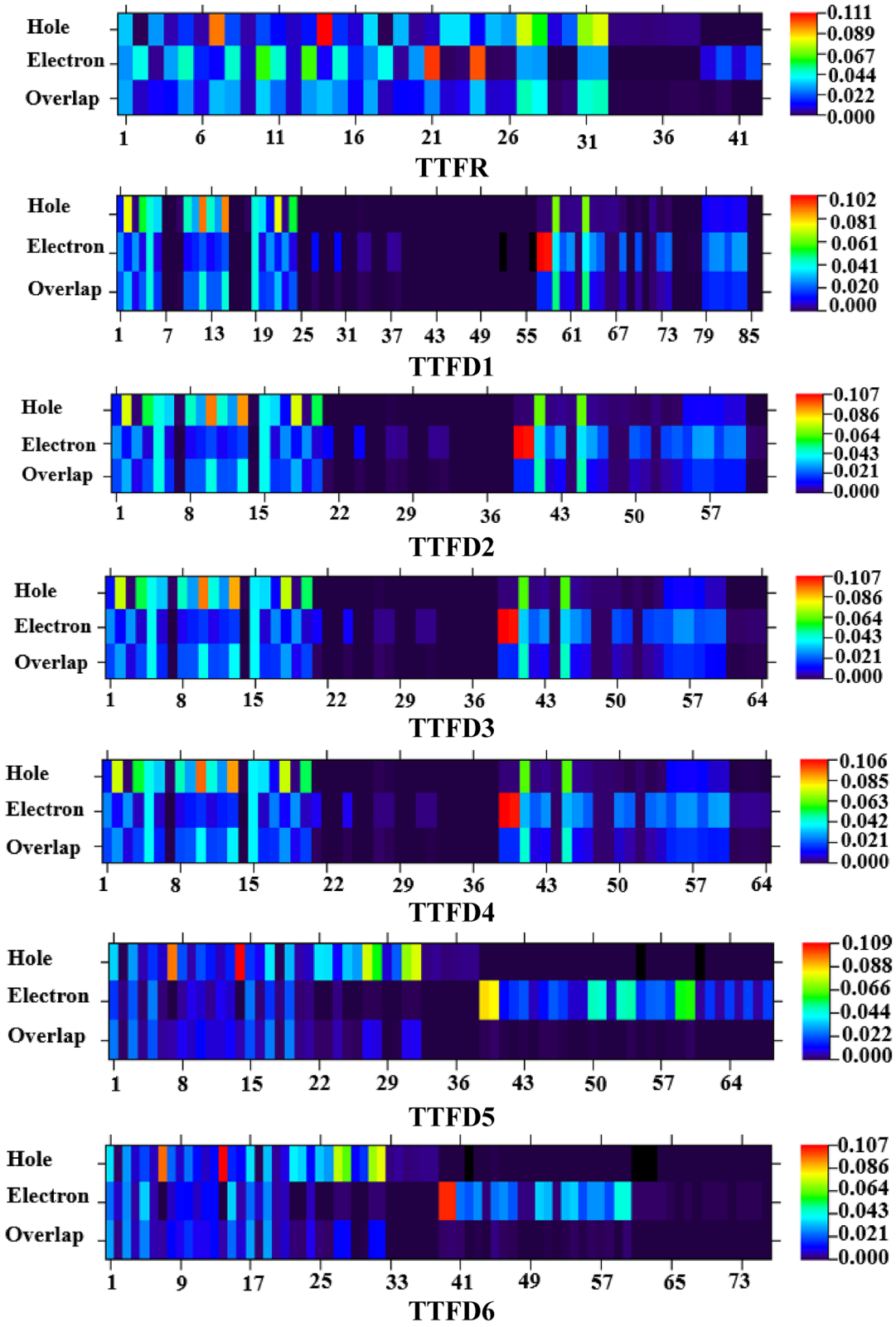

Figure 6. Pictorial illustration of hole-electron analysis for TTFR-TTFD6.

charge transference from HOMO to LUMO that was further supported by TDM and DOS analyses. TTFD5 exhibited the band gap value of 1.718 *eV* with significant reduction and highest absorption value of 897.071 *nm*, credited to the robust electron-withdrawing capability and prolonged conjugation of the terminal acceptor (A5). The open circuit voltage ranges between 1.771 and 1.789 *V* and the highest V_{oc} was determined to be 1.849 *V* for

Compounds	λ_e(eV)[a]	λ_h(eV)[b]
TTFR	0.00066671	-0.00059988
TTFD1	0.10532127	0.10506045
TTFD2	0.00010953	-0.00020501
TTFD3	0.00013195	-0.00033909
TTFD4	0.0001314	-0.00023788
TTFD5	-0.00001172	-0.00046074
TTFD6	-0.00007836	-0.00080507

Table 3. Reorganization energies (eV) of entitled compounds (TTFR-TTFD6). [a] reorganization energy of electron. [b] reorganization energy of hole.

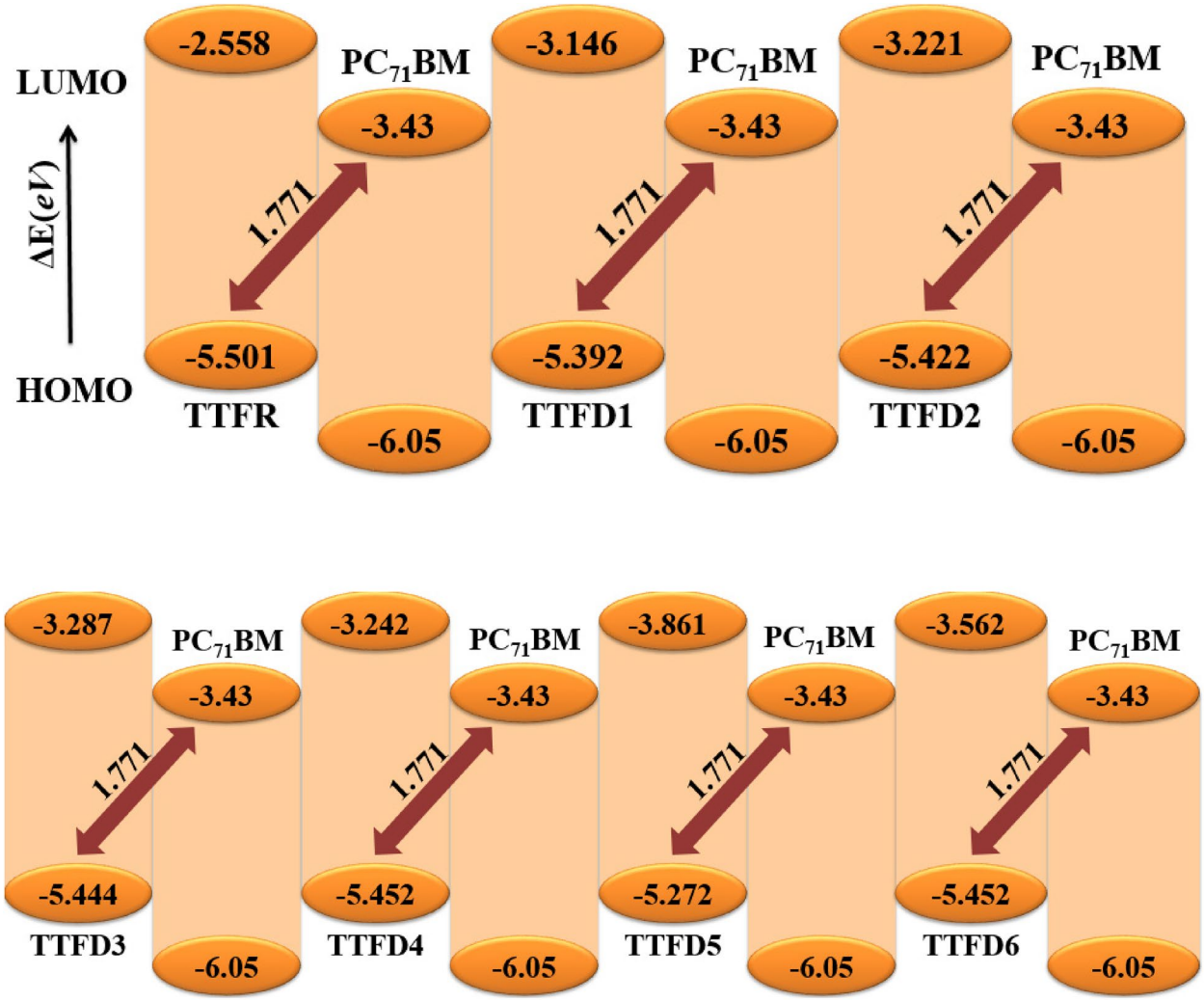

Figure 7. Diagrammatic representation of V_{oc} using $PC_{17}BM$ as the acceptor polymer.

TTFD5. The calculated binding energy (E_b) values for the derivatives (0.381 to 0.365 eV) were found to be less than that of the reference compound (0.394 eV), indicating good exciton dissociation rate. The descending order of E_b in all designed molecules is found as TTFR > TTFD2 > TTFD1 > TTFD4 > TTFD6 > TTFD5 > TTFD3. In short, aforesaid compounds attained by peripheral structural tailoring could be reasonable materials for OSCs, offering numerous desirable attributes in the future.

Computational procedure

Gaussian 09 software[63] was utilized to compute all the DFT/TD-DFT investigations in the TTFR and TTFD1-TTFD6 chromophores having A-π-A architecture. Gauss View 6.0[64] program was used to generate the input

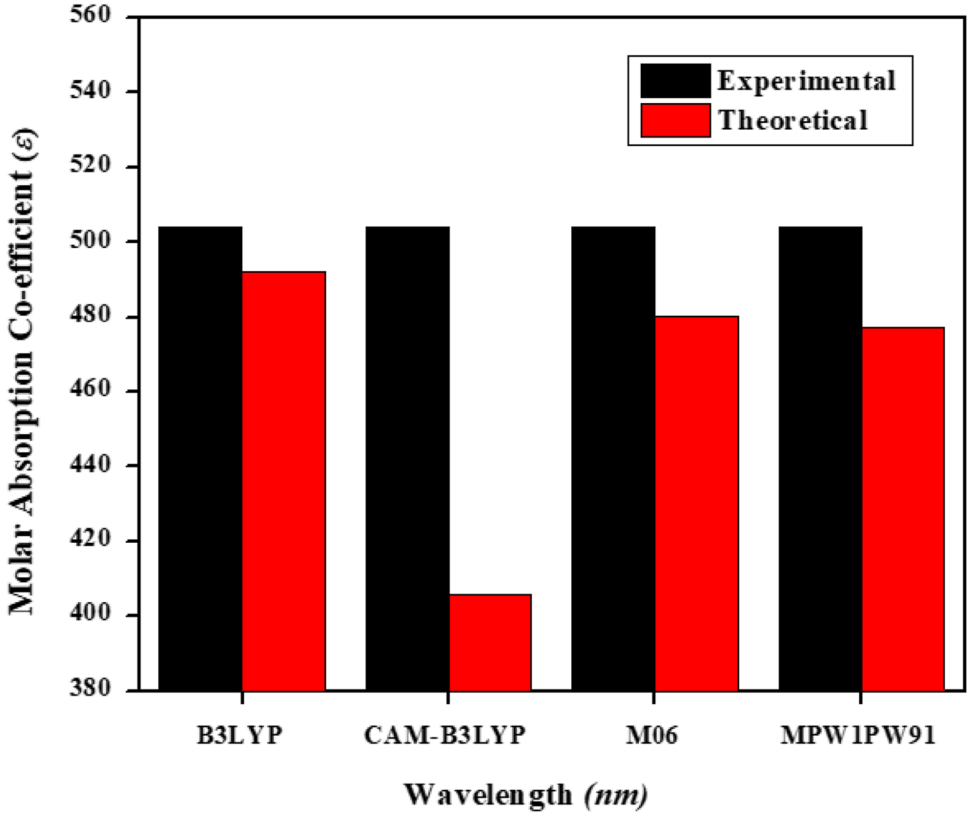

Figure 8. Comparison between theoretical and experimental UV-Visible results of TTFR in toluene solvent at various levels with 6-311G(d, p) basis set.

data and display the outcomes. To select the appropriate DFT level, the structural optimization of TTFR was conducted using four different levels: M06[65], B3LYP[66,67], CAM-B3LYP[68], and MPW1PW91[69], along with 6-311G(d, p) basis set in the toluene solvent.

After optimization, the simulated UV-Visible values of TTFR conducted in toluene solvent, resulting in λ_{max} values at aforementioned functionals: B3LYP (492.274 *nm*), CAM-B3LYP (477.193 *nm*), MPW1PW91 (405.840 *nm*) and M06 (480.335 *nm*) were compared with experimental (504 *nm*) results to select a suitable DFT functional for further study. The absorption spectrum from TD-DFT calculation using the B3LYP functional closely matched the experimental data as shown in the Table S8 and Fig. 8. Consequently, all the subsequent analyses were conducted at B3LYP/6-311G(d, p) functional to explore the optoelectronic and photovoltaic characteristics. To elucidate the effect of solvent on maximum absorption the conductor like polarizable continuum model (CPCM) was used.

The frontier molecular orbitals (FMOs), UV-Visible, density of state (DOS), transition density matrix (TDM), open circuit voltage (V_{oc}) and binding energy analyses were carried out for all the designed compounds at above mentioned functionals. Software such as Chemcraft[70], PyMOlyze[71], Multiwfn[72], Origin 8.0[73], and Avogadro[74], were utilized to extract the data in the forms of graphs and tables.

Data availability

All data generated or analyzed during this study are included in this published article and its supplementary information files.

Received: 11 May 2024; Accepted: 30 September 2024
Published online: 16 October 2024

References

1. Li, Y., Xu, G., Cui, C. & Li, Y. Flexible and semitransparent organic solar cells. *Adv. Energy Mater.* **8**, 1701791 (2018).
2. Meng, L. et al. Organic and solution-processed tandem solar cells with 17.3% efficiency. *Science.* **361**, 1094–1098 (2018).
3. Pintossi, D. et al. Luminescent downshifting by photo-induced sol-gel hybrid coatings: accessing multifunctionality on flexible organic photovoltaics via ambient temperature material processing. *Adv. Electron. Mater.* **2**, 1600288 (2016).
4. Lin, Y. et al. Self-assembled monolayer enables hole transport layer-free organic solar cells with 18% efficiency and improved operational stability. *ACS Energy Lett.* **5**, 2935–2944 (2020).
5. He, Z. et al. Simultaneous enhancement of open-circuit voltage, short-circuit current density, and fill factor in polymer solar cells. *Adv. Mater.* **23**, 4636–4643 (2011).
6. Menke, S. M. & Holmes, R. J. Exciton diffusion in organic photovoltaic cells. *Energy Environ. Sci.* **7**, 499–512 (2014).

7. Liu, T. & Troisi, A. What makes fullerene acceptors special as electron acceptors in organic solar cells and how to replace them. *Adv. Mater.* **25**, 1038–1041 (2013).
8. Khan, M. U. et al. Designing spirobifullerene core based three-dimensional cross shape acceptor materials with promising photovoltaic properties for high-efficiency organic solar cells. *Int. J. Quantum Chem.* **120**, e26377 (2020).
9. Lin, Y., Li, Y. & Zhan, X. Small molecule semiconductors for high-efficiency organic photovoltaics. *Chem. Soc. Rev.* **41**, 4245–4272 (2012).
10. Li, Y. Molecular design of photovoltaic materials for polymer solar cells: toward suitable electronic energy levels and broad absorption. *Acc. Chem. Res.* **45**, 723–733 (2012).
11. Chen, J. & Cao, Y. Development of novel conjugated donor polymers for high-efficiency bulk-heterojunction photovoltaic devices. *Acc. Chem. Res.* **42**, 1709–1718 (2009).
12. Yao, H. et al. Design, synthesis, and photovoltaic characterization of a small molecular acceptor with an ultra-narrow band gap. *Angew. Chem. Int. Ed.* **56**, 3045–3049 (2017).
13. Huang, C. et al. Highly efficient organic solar cells based on S, N-heteroacene non-fullerene acceptors. *Chem. Mater.* **30**, 5429–5434 (2018).
14. Holliday, S. et al. A rhodanine flanked nonfullerene acceptor for solution-processed organic photovoltaics. *J. Am. Chem. Soc.* **137**, 898–904 (2015).
15. Liu, Z. et al. Non-fullerene polymer acceptors based on perylene diimides in all-polymer solar cells. *Sol. Energy Mater. Sol. Cells.* **189**, 103–117 (2019).
16. Qi, Q. et al. Side-chain optimization of perylene diimide-thiophene random terpolymer acceptors for enhancing the photovoltaic efficiency of all-polymer solar cells. *Org. Electron.* **78**, 105616 (2020).
17. Wang, H. et al. Perylene diimide based star-shaped small molecular acceptors for high efficiency organic solar cells. *J. Mater. Chem. C.* **7**, 819–825 (2019).
18. Sariciftci, N. S., Smilowitz, L., Heeger, A. J. & Wudl, F. Photoinduced electron transfer from a conducting polymer to buckminsterfullerene. *Science*. **258**, 1474–1476 (1992).
19. Meng, D. et al. High-performance solution-processed non-fullerene organic solar cells based on selenophene-containing perylene bisimide acceptor. *J. Am. Chem. Soc.* **138**, 375–380 (2016).
20. Shafiq, I. et al. Introducing the various electron withdrawing functions in trigging the optical nonlinearity of benzodithiophene based chromophores: a quantum chemical approach. *J. Saudi Chem. Soc.* **27**, 101767 (2023).
21. Sharma, G., Mikroyannidis, J., Sharma, S. & Thomas, K. J. Bulk heterojunction organic photovoltaic devices based on small molecules featuring pyrrole and carbazole and 2-(4-nitrophenyl) acrylonitrile acceptor segments as donor and fullerene derivatives as acceptor. *Dyes Pigm.* **94**, 320–329 (2012).
22. Steinberger, S. et al. Vacuum-processed small molecule solar cells based on terminal acceptor-substituted low-band gap oligothiophenes. *Chem. Commun.* **47**, 1982–1984 (2011).
23. Lin, H. W. et al. An effective bilayer cathode buffer for highly efficient small molecule organic solar cells. *Org. Electron.* **13**, 1925–1929 (2012).
24. Hong, J. et al. All-small-molecule solar cells incorporating NDI-based acceptors: synthesis and full characterization. *ACS Appl. Mater. Interfaces*. **9**, 44667–44677 (2017).
25. Zhao, F. et al. Single-junction binary-blend nonfullerene polymer solar cells with 12.1% efficiency. *Adv. Mater.* **29**, 1700144 (2017).
26. Li, S. et al. Energy-level modulation of small-molecule electron acceptors to achieve over 12% efficiency in polymer solar cells. *Adv. Mater.* **28**, 9423–9429 (2016).
27. Ullah, H., Shah, A. H. A., Bilal, S. & Ayub, K. Doping and dedoping processes of polypyrrole: DFT study with hybrid functionals. *J. Phys. Chem. C.* **118**, 17819–17830 (2014).
28. Ullah, H., Bibi, S., Tahir, A. A. & Mallick, T. K. Density functional theory study of selenium-substituted low-bandgap donor–acceptor–donor polymer. *J. Phys. Chem. C.* **120**, 27200–27211 (2016).
29. Ullah, H., Shah, A. H. A., Bilal, S. & Ayub, K. DFT study of polyaniline NH3, CO2, and CO gas sensors: comparison with recent experimental data. *J. Phys. Chem. C.* **117**, 23701–23711 (2013).
30. Liu, Y. et al. Enhancing the performance of organic solar cells by hierarchically supramolecular self-assembly of fused-ring electron acceptors. *Chem. Mater.* **30**, 4307–4312 (2018).
31. Li, L., Yan, B., Yang, J., Chen, L. & Zeng, H. Novel mussel-inspired injectable self-healing hydrogel with anti-biofouling property. *Adv. Mater. (Deerfield Beach Fla).* **27**, 1294–1299 (2015).
32. Wang, R. et al. Rational tuning of molecular interaction and energy level alignment enables high-performance organic photovoltaics. *Adv. Mater.* **31**, 1904215 (2019).
33. Huang, H. et al. Noncovalently fused-ring electron acceptors with near-infrared absorption for high-performance organic solar cells. *Nat. Commun.* **10**, 3038 (2019).
34. Ullah, H., Bibi, S., Tahir, A. A. & Mallick, T. K. Donor-acceptor polymer for the design of all-solid-state dye-sensitized solar cells. *J. Alloys Compd.* **696**, 914–922 (2017).
35. Watts, K. E. et al. Stability of push–pull small molecule donors for organic photovoltaics: spectroscopic degradation of acceptor endcaps on benzo [1, 2-b: 4, 5-b′] dithiophene cores. *J. Mater. Chem. A.* **7**, 19984–19995 (2019).
36. Giribabu, L. et al. Stable and charge recombination minimized π-extended thioalkyl substituted tetrathiafulvalene dye-sensitized solar cells. *Mater. Chem. Front.* **1**, 460–467 (2017).
37. Henke, P. et al. Imparting Stability to Organic Photovoltaic Components through Molecular Engineering: mitigating reactions with Singlet Oxygen. *ChemSusChem*. **16**, e202202320 (2023).
38. Wang, J. et al. A perylene-based Polycyclic Aromatic Hydrocarbon Electron Donor for a highly efficient solar cell dye. *ChemSusChem*. **10**, 2962–2967 (2017).
39. Liao, C. et al. Green solvent-processed efficient non-fullerene organic solar cells enabled by low-bandgap copolymer donors with EDOT side chains. *J. Mater. Chem. A*. **7**, 716–726 (2019).
40. MacDiarmid, A. G. Nobel lecture:synthetic metals: a novel role for organic polymers. *Rev. Mod. Phys.* **73**, 701 (2001).
41. Akram, S. J. et al. Impact of various heterocyclic π-linkers and their substitution position on the opto-electronic attributes of the A–π–D–π–A type IECIO-4F molecule: a comparative analysis. *RSC Adv.* **12**, 20792–20806 (2022).
42. Haq, S. et al. Transmittal Effect Evaluation of Heterocyclic Rings on Nonlinear Optical Ambit of Benzotrithiophene-Based Push-Pull Driving Materials: a Theoretical Approach. Polycycl. *Aromat. Compd.* **44**, 5338–5361 (2023).
43. Wielopolski, M. et al. Position-dependent extension of π-conjugation in D-π-A dye sensitizers and the impact on the charge-transfer properties. *J. Phys. Chem. C.* **117**, 13805–13815 (2013).
44. Hussain, R. et al. Enhancement in photovoltaic properties of N, N-diethylaniline based donor materials by bridging core modifications for efficient solar cells. *ChemistrySelect*. **5**, 5022–5034 (2020).
45. Shafiq, I. et al. The influence of selenophene π-linker on photovoltaic properties of pyrrole-4, 6 (5-H)-dione-based chromophores: A quantum chemical study. *J. Ind. Eng. Chem.* **136**, 589–602 (2024).
46. Chen, C. P., Chan, S. H., Chao, T. C., Ting, C. & Ko, B. T. Low-bandgap poly (thiophene-phenylene-thiophene) derivatives with broaden absorption spectra for use in high-performance bulk-heterojunction polymer solar cells. *J. Am. Chem. Soc.* **130**, 12828–12833 (2008).
47. Shafiq, I. et al. Exploration of the synergistic effect of chrysene-based core and benzothiophene acceptors on photovoltaic properties of organic solar cells. *Sci. Rep.* **14**, 15105 (2024).

48. Mainville, M. et al. Theoretical insights into optoelectronic properties of non-fullerene acceptors for the design of organic photovoltaics. *ACS Appl. Energy Mater.* **4**, 11090–11100 (2021).
49. Jabeen, S., Khera, R. A., Iqbal, J. & Asgher, M. Design, synthesis and application of triazole ligands in suzuki miyaura cross coupling reaction of aryl chlorides. *J. Mol. Struct.* **1206**, 127753 (2020).
50. Khalid, M. et al. Efficient tuning of small acceptor chromophores with A1-π-A2-π-A1 configuration for high efficacy of organic solar cells via end group manipulation. *J. Saudi Chem. Soc.* **25**, 101305 (2021).
51. Abbas, F. et al. An optoelectronic study to design better benzodithiophene (BDT) donor unit based non-fullerene organic solar cells (OSCs): the DFT approaches. *Chem. Pap.* **76**, 4977–4987 (2022).
52. Li, Y. & Ullrich, C. Time-dependent transition density matrix. *Chem. Phys.* **391**, 157–163 (2011).
53. Hassan, T. et al. Development of non-fused acceptor materials with 3D-Interpenetrated structure for stable and efficient organic solar cells. *Mater. Sci. Semiconduct. Process.* **151**, 107010 (2022).
54. Clarke, T. M. & Durrant, J. R. Charge photogeneration in organic solar cells. *Chem. Rev.* **110**, 6736–6767 (2010).
55. Correa-Baena, J. P. et al. A-site cation in inorganic A 3Sb2I9 perovskite influences structural dimensionality, exciton binding energy, and solar cell performance. *Chem. Mater.* **30**, 3734–3742 (2018).
56. Shafiq, I. et al. Influence of benzothiophene acceptor moieties on the non-linear optical properties of pyreno-based chromophores: first-principles DFT framework. *RSC Adv.* **14**, 15964–15978 (2024).
57. Liu, Z., Wang, X., Lu, T., Yuan, A. & Yan, X. Potential optical molecular switch: Lithium@ cyclo [18] carbon complex transforming between two stable configurations. *Carbon*. **187**, 78–85 (2022).
58. Mogensen, J. et al. Indenofluorene-extended tetrathiafulvalene scaffolds for Dye-Sensitized Solar cells. *Eur. J. Org. Chem.* **2020**, 6127–6134 (2020).
59. Ali, U., Tariq, A., Kiran, A., Abbas, F. & Khalil, M. T. Tuning the absorption and optoelectronic properties of naphthalene diimide based solar cells with non-fullerene acceptors. *Chem. Pap.* **75**, 4327–4336 (2021).
60. Li, S. et al. An unfused-core-based nonfullerene acceptor enables high-efficiency organic solar cells with excellent morphological stability at high temperatures. *Adv. Mater.* **30**, 1705208 (2018).
61. Wu, Z., Fan, B., Xue, F., Adachi, C. & Ouyang, J. Organic molecules based on dithienyl-2, 1, 3-benzothiadiazole as new donor materials for solution-processed organic photovoltaic cells. *Sol. Energy Mater. Sol. Cells*. **94**, 2230–2237 (2010).
62. Scharber, M. C. et al. Design rules for donors in bulk-heterojunction solar cells—towards 10% energy-conversion efficiency. *Adv. Mater.* **18**, 789–794 (2006).
63. Frisch, M. et al. Other. Gaussian 09, Gaussian, Inc. *Wallingford CT*. **32**, 5648–5652 (2009).
64. Dennington, R., Keith, T. A. & Millam, J. M. *GaussView 6.0. 16* 143–150 (Semichem Inc : Shawnee Mission KS, USA, 2016).
65. Bryantsev, V. S., Diallo, M. S., Van Duin, A. C. & Goddard, I. I. I. Evaluation of B3LYP, X3LYP, and M06-class density functionals for predicting the binding energies of neutral, protonated, and deprotonated water clusters. *J. Chem. Theory Comput.* **5**, 1016–1026 (2009).
66. Civalleri, B., Zicovich-Wilson, C. M., Valenzano, L. & Ugliengo, P. B3LYP augmented with an empirical dispersion term (B3LYP-D*) as applied to molecular crystals. *CrystEngComm*. **10**, 405–410 (2008).
67. Strati, G. L., Willett, J. L. & Momany, F. A. A DFT/ab initio study of hydrogen bonding and conformational preference in model cellobiose analogs using B3LYP/6-311++G. *Carbohydr. Res.* **337**, 1851–1859 (2002).
68. Yanai, T., Tew, D. P. & Handy, N. C. A new hybrid exchange–correlation functional using the Coulomb-attenuating method (CAM-B3LYP). *Chem. Phys. Lett.* **393**, 51–57 (2004).
69. Adamo, C. & Barone, V. Exchange functionals with improved long-range behavior and adiabatic connection methods without adjustable parameters: the m PW and m PW1PW models. *J. Chem. Phys.* **108**, 664–675 (1998).
70. Zhurko, G. & Zhurko, D. *ChemCraft version 1.6* (2009)http://www.chemcraftprog.com.
71. O'boyle, N. M., Tenderholt, A. L. & Langner, K. M. Cclib: a library for package-independent computational chemistry algorithms. *J. Comput. Chem.* **29**, 839–845 (2008).
72. Lu, T., Chen, F. & Multiwfn A multifunctional wavefunction analyzer. *J. Comput. Chem.* **33**, 580–592 (2012).
73. Stevenson, K. J. Review of originpro 8.5. *J. Am. Chem. Soc.* **133**, 5621 (2011).
74. Hanwell, M. D. et al. Avogadro: an advanced semantic chemical editor, visualization, and analysis platform. *J. Cheminform.* **4**, 1–17 (2012).

Acknowledgements

Dr. Muhammad Khalid gratefully acknowledges the financial support of HEC Pakistan (project no. 20-14703/NRPU/R&D/HEC/2021). Authors are thankful for cooperation and collaboration of A.A.C.B from IQ-USP, Brazil especially for his continuous support and providing computational lab facilities. A.A.C.B. (grant 2015/01491-3) is highly thankful to Fundação de Amparo à Pesquisa do Estado de São Paulo for the cooperation and financial assistance. The authors thank the Researchers Supporting Project number (RSPD2024R644), King Saud University, Riyadh, Saudi Arabia. S.C.O. acknowledges the support from the doctoral research fund of the Affiliated Hospital of Southwest Medical University.

Author contributions

M.K.: Supervision; Investigation; Resources; software; project administration; MethodologyA.T.: Formal analysis; Investigation; Writing - original draft; VisualizationA.A.C.B.: Conceptualization; Resources; software; Formal analysis; ValidationR.A.: Data Curation; Writing - review & editing; Formal analysis, Funding acquisitionS.C.O.: Formal analysis; Investigation; Writing - review & editing; Funding acquisition; Visualization.

Declarations

Competing interests

The authors declare no competing interests.

Additional information

Supplementary Information The online version contains supplementary material available at https://doi.org/10.1038/s41598-024-74852-0.

Correspondence and requests for materials should be addressed to M.K. or S.C.O.